Pressure-induced charge ordering transition in $CaMn_7O_{12}$

M. Stekiel,[1,2] A. Girard,[1,3] D. Zimmer,[1] V. Monteseguro,[4] K. Glazyrin,[5] I. de Pedro,[4] L. Bayarjargal,[1] B. Winkler,[1] and J. Ruiz-Fuertes[4,*]

[1]*Institute of Geosciences, University of Frankfurt, Altenhoeferallee 1, Frankfurt am Main 60438, Germany*
[2]*Physik Department, Technische Universität München, James-Franck-Strasse 1, Garching 85748, Germany*
[3]*Sorbonne Université, CNRS UMR8233, MONARIS, 4 place Jussieu, 75005 Paris, France*
[4]*DCITIMAC, Universidad de Cantabria, Avenida Los Castros 48, 39005 Santander, Spain*
[5]*Deutsches Elektronen-Synchrotron DESY, Notkestrasse 85, 22603 Hamburg, Germany*

(Received 16 November 2021; revised 19 January 2022; accepted 15 February 2022; published 25 February 2022)

We use high-pressure resistivity and single crystal x-ray diffraction at ambient and low temperature to investigate the charge ordering phase transition of $CaMn_7O_{12}$. We have found that at ambient temperature the Jahn-Teller distortion of the $Mn^{3+}O_6$ octahedra rapidly decreases above 20 GPa, and vanishes at 28 GPa, when two Mn octahedral sites initially occupied by Mn^{3+} and Mn^{4+} become regular and equivalent as the result of a charge delocalization. Such a change correlates with a two orders of magnitude drop in the resistivity and a symmetry increase from the low-pressure rhombohedral $R\bar{3}$ phase to the cubic $Im\bar{3}$ structure, the same as one found at ambient pressure above 440 K. This yields the slope of the charge ordering phase boundary of $dT_c/dp \approx -6$ K/GPa. This result is further supported by the lack of a structural phase transition up to the maximum measured pressure of 30 GPa when the experiment is performed at 70 K. The satellite reflections of the structural modulation of the multiferroic phase of $CaMn_7O_{12}$ observed at 70 K were found to hold up to 25 GPa with the structure keeping a constant modulation vector $k = (0\ 0\ 0.925)$ with pressure. The average structure at 70 K does not show other indications of further phase transition.

DOI: 10.1103/PhysRevB.105.064110

I. INTRODUCTION

With a spin-induced spontaneous ferroelectric polarization of 2870 $\mu C\,m^{-2}$ below 90 K [1–4], a large negative thermal expansion in the 425–490 K range [5], a strong orbital-lattice coupling, an insulator to semimetal transition [6] at 425 K, and a Mn^{3+}/Mn^{4+} (nominal $Mn^{3.25+}$) charge ordering occurring at 425 K mixed-valence $CaMn_7O_{12}$ is a promising candidate in next generation ultrafast electronic devices [7–9].

The source of these interesting properties is the crystal structure of $CaMn_7O_{12}$, where different bonding schemes for Mn-O are realized, and various types of phase transitions occur across temperature. At ambient temperature $CaMn_7O_{12}$ crystallizes in a quadruple-perovskite-type structure, described with a rhombohedral space group $R\bar{3}$. In this structure Mn occupies three different crystallographic sites: Mn1 site coordinated by four oxygens in a square planar geometry, and two octahedral sites, Mn2 and Mn3, coordinated by six oxygen atoms [6,10], as shown in Fig. 1. Both octahedral sites are close to being equivalent but due to the different valence of Mn in $CaMn_7O_{12}$ at ambient temperature, those with Mn^{4+} (Mn3) present a perfect octahedral coordination (O_h), while the remaining octahedra sites (Mn2) occupied by Mn^{3+} are distorted in a rare apical-contracted D_{4h} symmetry due to the Jahn-Teller effect. The distortion quenching could possibly lead to a symmetry equivalence of the Mn2 and Mn3 sites and therefore to an overall symmetry increase. Unveiling the subtle contribution that the Jahn-Teller effect has on the crystal structure of $CaMn_7O_{12}$ requires a precise determination of its structure as a function of the interatomic distances. This is particularly relevant since optical absorption spectroscopy cannot be employed to access the Mn $d \rightarrow d^*$ crystal-field transitions in a material with a predicted band gap of 240 meV [11].

Structure and properties of $CaMn_7O_{12}$ have been widely studied as a function of temperature [6,11–13]. It undergoes a first-order phase transition in the temperature range 400–460 K as evidence by phase separation [14]. It is accompanied by a drop in the resistivity of more than one order of magnitude [6]. This transition is associated with the closure of its band gap [11] and a symmetry increase from rhombohedral $R\bar{3}$ to a cubic with space group $Im\bar{3}$, both of which are shown Fig. 1. Such a phase transition is controlled by a charge ordering [5] concomitant with the symmetry equivalence of the Mn2 and Mn3 sites. Upon heating, the distortion of the $Mn^{3+}O_6$ octahedra (Mn2 site) does not change in the mixed-phase region [14] around 440 K. At low temperatures $CaMn_7O_{12}$ undergoes a series of phase transitions associated with the structural modulations that affect the Mn-O bond lengths [15], induce orbital ordering [2,3], and produce the onset of incommensurate magnetic ordering closely connected with the structural modulation [2,13,15]. On the other hand, the behavior of $CaMn_7O_{12}$ upon compression has not been studied.

*ruizfuertesj@unican.es

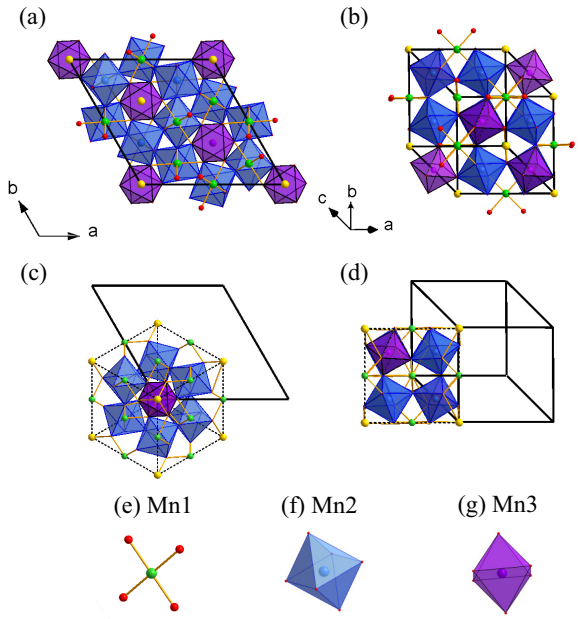

FIG. 1. Crystal structure of $CaMn_7O_{12}$ at ambient conditions. (a) and (b) The hexagonal unit cell along the [0 0 1] and [1 $\bar{1}$ 2] directions, respectively. (c) and (d) The structure limited to the cubic unit cell indicated with a dashed line, which represents the structure at high temperature, in the same view as (a) and (b), respectively. The hexagonal unit cell is shown with a solid line. Mn atoms occupy three distinct sites with different Mn-O bonding schemes: (e) $Mn^{3+}O_4$ in square planar configuration, (f) $Mn^{3+}O_6$ distorted octahedra, and (g) $Mn^{4+}O_6$ regular octahedra.

Considering that transformations under high pressure reduce the structural fluctuations [16], inducing the same phase transition under compression in $CaMn_7O_{12}$ would help to unveil the interplay between the Jahn-Teller effect and the charge ordering. $Im\bar{3}$ space group is a translationengleiche supergroup of $R\bar{3}$ with both structures keeping a large degree of similarity (Fig. 1). Although the first order nature of this phase transition is confirmed by a coexistence of both phases in a 65 K wide temperature range [14], this type of phase transition with a strong displacive character commonly follows the same structural route either by heating or by applying pressure [17,18].

In order to unveil the interplay between the Mn^{3+} Jahn-Teller effect and the charge ordering in $CaMn_7O_{12}$ along its phase transition we have induced it under high pressure and studied its effects by means of resistivity and single-crystal x-ray diffraction measurements (SXRD) at ambient temperature. We have also performed high-pressure SXRD measurements at 70 K in order to follow the evolution of various ordering mechanisms of the ferroelectric $CaMn_7O_{12}$ induced by strong magnetoelastic coupling.

II. EXPERIMENTAL METHODS

$CaMn_7O_{12}$ single crystals were grown following the flux method of Johnson *et al.* [2] in which a 5 g mixture of $CaCl_2$:MnO_2 was heated for 24 h in an alumina crucible in air at 850 °C, and then cooled down.

High-pressure experiments were carried out using Boehler-Almax [19] diamond-anvil cells (DACs) with diamonds with 350 μm culets. Three single crystals of $CaMn_7O_{12}$ with approximate thicknesses of 10 μm were loaded in three large-opening DACs. The pressure chamber was formed in a 130 μm diameter hole in rhenium gaskets preindented to a thickness of 40 μm. Ruby chips were also loaded for pressure determination [20]. Helium was employed as a hydrostatic pressure-transmitting medium. The SXRD experiments both at 293 and 70 K were performed at the P02.2 Extreme Conditions beamline [21] at PETRA-III synchrotron using a wavelength of 0.2909 Å focused down to $3 \times 8\ \mu m^2$ (FWHM) and a PerkinElmer detector placed at 400 mm from the sample. The diffraction images were collected every 0.5° in ω scans and the reflections were indexed, integrated, and scaled using the CrysAlisPro software [22]. The scaling procedure corrects for various effects modifying the diffracted reflections' intensity, such as angle-dependent absorption of the beam on diamond anvils, reduction in the beam intensity due to fulfilling Laue condition for the top diamond, and sample shape. For the experiment at 70 K the DAC was placed inside a modified cold-finger cryostat from Oxford Instruments described elsewhere [21]. The structure at different pressures was solved using SHELXT [23] and refined using SHEXL [24].

The resistivity of $CaMn_7O_{12}$ was determined as a function of pressure using a four-wire connection resistance measurements in a diamond-anvil cell. Four gold wires were used to establish contact between the multimeter (DMM7510, Keithley) and a single crystal of $CaMn_7O_{12}$. The wires lying on the diamond anvil were pressed against a sample embedded in a mixture of epoxy resin and aluminum oxide on the other side [25]. This mixture insulates the sample and wires from the tungsten gasket and acts as the pressure-transmitting medium. The epoxy-aluminum oxide is a nonhydrostatic pressure medium, which can introduce pressure gradients across the sample, however, our preparation method does not seem to substantially influence the transition width, as evidence by our calibration in [26]. Possible errors due to thermoelectric effects were avoided by alternating the direction of the current.

Further details on sample preparation can be provided by authors upon request.

III. RESULTS AND DISCUSSION

A. Resistivity at high pressures and ambient temperature

The pressure dependence of the resistivity of $CaMn_7O_{12}$ is shown in Fig. 2. Based on the rate of change of resistivity, it can be roughly divided into three regions as indicated by the vertical lines positioned at 17.5 and 27 GPa, and illustrated in the inset, where the log-derivative of resistivity is plotted as the function of pressure. For pressures below 17.5 GPa there is a stable decrease of resistivity, afterwards it falls by three orders of magnitude up to the pressure of 28 GPa, above which it does not change significantly. The nonhydrostaticity of the pressure medium can introduce pressure gradients across the sample and a uniaxial stress. We have estimated the former one by the width of the ruby fluorescence line and adapted

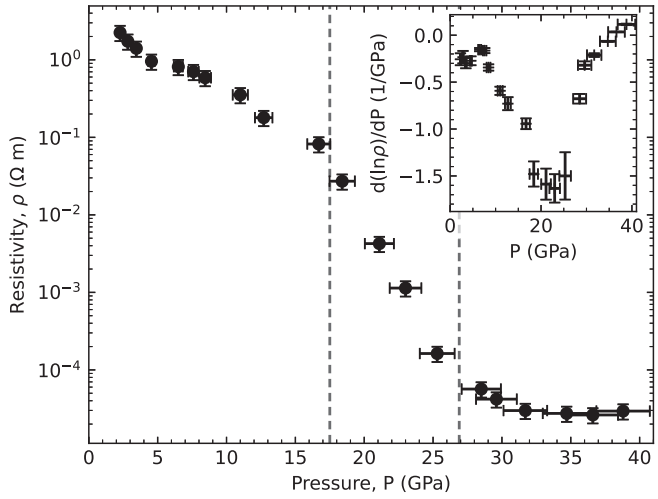

FIG. 2. Ambient temperature pressure dependence of the resistivity ρ of $CaMn_7O_{12}$ as measured by the four-probe method. The inset presents the pressure derivative of the $\ln(\rho)$ as a function of pressure, which illustrates that, based on the rate of resistivity change, it can be divided into three regions as indicated by the vertical line in the main plot, and discussed in the main text.

the pressure error bars accordingly, as shown in Fig. 2. Significant increase in pressure gradient was observed above 20 GPa, which is connected to the opening of the gasket, see Fig. S1. Nevertheless, we did not observe any pressure loss up to 39 GPa, the maximum pressure reached. An attempt to further increase the pressure resulted in losing the connection to the sample, as the golden wires were cut by the gasket and the resistivity could not be measured upon pressure release. The presence of the uniaxial stress cannot be excluded, and the analysis of the results should involve such possibility.

Similar features in resistivity were observed in $CaMn_7O_{12}$ across the transition at 425 K and ambient pressure in single crystals [6] and thin films [11], where the region of the resistivity drop corresponds to the $R\bar{3} \rightarrow Im\bar{3}$ phase transition and charge delocalization. This suggests that a similar transition could be observed at high pressure.

B. Crystal structure at high pressure

1. X-ray diffraction at ambient temperature

At ambient temperature, the reflections were successfully indexed with the rhombohedral space group $R\bar{3}$ up to 35 GPa, the maximum pressure reached, and the data quality allowed for a reliable structural refinement. Due to geometrical restrictions of the diamond-anvil cell, the number of reflections did not allow for simultaneous refinement of anisotropic displacement parameters for all atoms. A careful inspection of the oxygen displacement parameters at all pressures shows that they are close to the values for other atoms and scale with atomic masses. At 25.5 GPa, where they differ most, the isotropic displacement of O atoms is 0.0125(4) and 0.0114(3) $Å^2$, while those of Mn is 0.0080(2) $Å^2$ and Ca is 0.0090(3) $Å^2$. This denies a possibility of positional disorder of O atoms, and reinforces the fact that $CaMn_7O_{12}$ accommodates the unusual, contracted Jahn-Teller distortion, which was wrongly determined for other ferrodistortive perovskites [27,28].

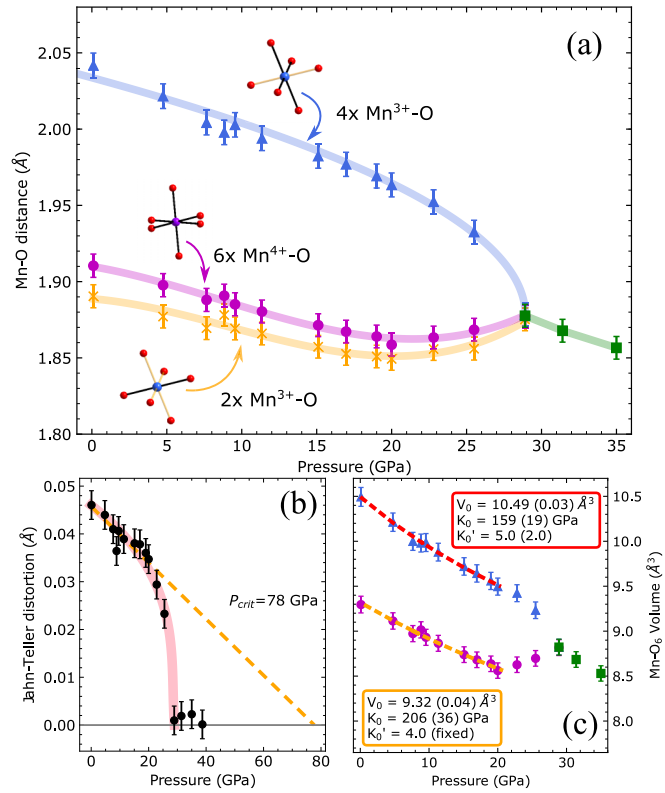

FIG. 3. (a) Pressure dependence of the Mn^{3+}-O and Mn^{4+}-O distances of $CaMn_7O_{12}$ at ambient temperature. The four long Mn^{3+}-O, the two short Mn^{3+}-O, and the six Mn^{4+}-O distances are represented by triangles, crosses, and circles, respectively, when refined with the $R\bar{3}$ space group. The regularized Mn-O distances, refined in the $Im\bar{3}$ space group, are shown with squares. (b) Pressure evolution of the Jahn-Teller distortion of the $Mn^{3+}O_6$ octahedra, together with the linear extrapolation of the distortion only from the data up to 20 GPa (dashed line). (c) $Mn^{3+}O_6$ (triangles) and $Mn^{4+}O_6$ (circles) octahedral volume change with pressure in the rhombohedral phase, and the volume of regular octahedra (squares) in the cubic phase. The fit is done with a third- ($Mn^{3+}O_6$) or second- ($Mn^{4+}O_6$) order BM EoS and its range is shown with a dashed line, while the fitted values are shown in the box. In all panels solid lines are guides for the eye.

The most apparent change in the crystal structure of $CaMn_7O_{12}$ upon applying pressure is the change of the Mn-O bond distances in the MnO_6 octahedra, as shown in Fig. 3. Up to 20 GPa the Mn-O octahedral distances decrease linearly with pressure at different rates. The six equivalent Mn^{4+}-O and the two short Mn^{3+}-O distances decrease at a rate around −0.002 Å/GPa, while the four long Mn^{3+}-O distances decrease twice faster at −0.004 Å/GPa. Such a different compression rate of the Mn^{3+}-O distances reduces the Jahn-Teller distortion, defined here as the average difference between the individual and mean Mn^{3+}-O bond lengths [29], from 0.046 Å at ambient pressure to 0.034 Å at 20 GPa, as shown in Fig. 3(b). The linear extrapolation to higher pressures shows that the $Mn^{3+}O_6$ octahedra would become regular at 78 GPa. This contrasts with the high temperature behavior, where the Mn-O bond lengths remain unchanged [14]. Above 20 GPa the long Mn^{3+}-O distance starts to rapidly decrease

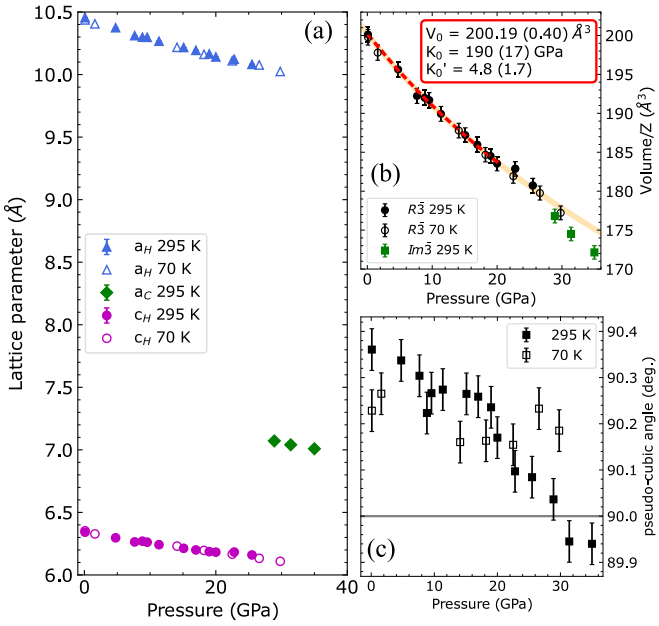

FIG. 4. (a) Evolution of lattice parameters of $CaMn_7O_{12}$ with pressure at ambient temperature (full symbols) and 70 K (open symbols). Triangles and circles denote the a and c parameters of the rhombohedral $R\bar{3}$ space group, while diamonds show the lattice parameter a of the cubic phase $Im\bar{3}$ after the phase transition. (b) Pressure dependence of the unit cell volume, following the convention in (a). The third-order BM EoS was fit to the 295 K data in the range indicated by the dashed, red line and extrapolated to higher pressures, as shown with the solid, orange line. The fit values are shown in the box. (c) Pseudocubic angle α_c at ambient temperature (solid squares) and 70 K (empty squares) that quantifies the level of rhombohedral distortion from the cubic lattice, for which $\alpha_c = 90^\circ$.

and the short Mn^{3+}-O distance increases, so that they become equal at 28 GPa and the Jahn-Teller distortion is suppressed. These pressures 20 and 28 GPa coincide with the beginning and ending of the resistivity drop shown before in Fig. 2, even though a nonhydrostatic pressure medium was used for resistivity measurements. As a result, above 28 GPa the structure consist only of regular MnO_6 octahedra, thus resembling the high temperature, cubic structure with the $Im\bar{3}$ space group. The level of distortion of the $R\bar{3}$ from the $Im\bar{3}$ structure can be quantified by evaluating the pseudocubic angle α_c from the rhombohedral lattice parameters [31] for which $\alpha_c \neq 90^\circ$ for rhombohedral lattice and $\alpha_c = 90^\circ$ for cubic lattice. As shown in Fig. 4(c), below 20 GPa α_c is $\approx$90.28° while above 20 GPa it decreases to 90° and stabilizes at this value above 28 GPa, within the experimental error.

Given the regularization of all MnO_6 octahedra at high pressure, an increase of the symmetry to the cubic $Im\bar{3}$ was considered. The refinement with the $Im\bar{3}$ space group was convergent for all data sets, but had lower figure of merit R_1 for measurements above 28 GPa, see Table I and Fig. S2 in [30]. Thus, we conclude that a structural phase transition occurs at 28 GPa with a change of space group from $R\bar{3}$ to $Im\bar{3}$. It is coincident with the regularization of the Jahn-Teller distorted $Mn^{3+}O_6$ octahedra and the resistivity drop.

Considering the compressibility of the lattice parameters at ambient temperature in Fig. 4(a), even though the a axis is

TABLE I. Details of structure solution and refinement at selected pressures and temperatures. In the second column, to facilitate comparison, arrows indicate values obtained by transforming back the parameters refined with constrains given by $Im\bar{3}$ space group. For more details see the Supplemental Material [30].

	$Im\bar{3}$	$R\bar{3}$	$R\bar{3}$
Pressure	28.9 GPa	28.9 GPa	29.8 GPa
Temperature	300 K	300 K	70 K
No. refined refl.	197	317	326
R_{int}	6.82%	3.68%	4.48%
h	−13 : 12	−16 : 14	−17 : 20
k	−11 : 11	−17 : 20	−17 : 14
l	−9 : 9	−6 : 7	−7 : 6
a	7.072 Å → 10.001 Å	10.000 Å	10.024 Å
c	7.072 Å → 6.124 Å	6.118 Å	6.109 Å
V	353.62 Å^3 → 530.43 Å^3	529.90 Å^3	531.65 Å^3
Z	2	3	3
O1(x)	0.3074 → 0.2234	0.2234	0.2238
O1(y)	0.1814 → 0.2654	0.2652	0.2707
O1(z)	0 → 0.084	0.0843	0.0817
O2(x)	– → 0.3518	0.3516	0.3464
O2(y)	– → 0.5222	0.52192	0.5228
O2(z)	– → 0.3408	0.3405	0.3420
No. parameters	13	37	30
R_1	8.37%	9.42%	8.77%

65% longer than the c axis, their linear compressibility is similar, -1.37×10^{-3} and -1.11×10^{-3} GPa^{-1}, respectively. Regarding the unit cell volume, the V-P data of the rhombohedral phase before the phase transition were fit with the third-order Birch-Murnaghan (BM) equation of state (EoS) [32], as shown with a dashed line in Fig. 4(b), yielding the bulk modulus $K_0 = 190(17)$ GPa. The extrapolation of the fitted EoS to higher pressures shows that the compressibility of $CaMn_7O_{12}$ above 28 GPa is not accurately described with the EoS with the same parameters, see solid line in Fig. 4(b), and implies a larger compressibility of the cubic phase, since the points lie below the extrapolated line. Unfortunately, due to the low number of data points above the transition, obtaining a reliable bulk modulus of the cubic phase is not possible. Increase in compressibility is quite unexpected for high-pressure structural transitions, however, a recent study on ScF_3 reports such an effect in a broad temperature range. This can also indicate a structural instability and point to a further phase transition at approaching pressures.

Owing to the high quality of the obtained data on the crystal structure, we are also able to follow the compressibility of the distinct $Mn^{3+}O_6$ and $Mn^{4+}O_6$ octahedra. As shown in Fig. 3(c), the bulk modulus of the regular $Mn^{4+}O_6$ octahedra $K_0 = 206$ GPa is higher than that of the distorted $Mn^{4+}O_6$ octahedra $K_0 = 159$ GPa. After the transition to the cubic phase, all MnO_6 become equivalent and regular, and show different volume than before the transition. Interestingly, by employing the method of Aguado *et al.* [33], we are able to determine the Jahn-Teller energy associated with the distortion of the $Mn^{3+}O_6$ octahedra, which is usually determined with optical spectroscopy methods, but is inaccessible in $CaMn_7O_{12}$ given an activation energy 190–240 meV and band gap of

240 meV [11]. Given the $K_0 = 159$ GPa for the $Mn^{3+}O_6$ octahedra and a critical pressure of 78 GPa, Jahn-Teller energy is $E_{JT} = 0.46$ meV, which is larger than for MnO_6 octahedra in $LaMnO_3$, where $E_{JT} = 0.25$ eV, and similar to the values determined for MnF_6 octahedra ranging between 0.26–0.48 eV for different compounds [34].

The question about the mechanism of the high-pressure transition in $CaMn_7O_{12}$ may be answered by comparative overview with the high-temperature phase transition in $CaMn_7O_{12}$. At 440 K $CaMn_7O_{12}$ undergoes similar $R\bar{3} \rightarrow Im\bar{3}$ transition, with regularization of MnO_6 octahedra [14]. The transition is clearly of first order, as evidenced by a separation of $R\bar{3}$ and $Im\bar{3}$ phases in the temperature range 400–460 K, based on reflections splitting in the x-ray diffractograms. In the current high-pressure study we have not observed any sign of reflection splitting, see the Supplemental Materials Fig. S2 [30], and the refined structure shows smooth evolution of interatomic lengths, see Fig. 3, suggesting a displacive character of the transition, which progresses between 20 and 28 GPa. At the same time we have observed a very similar dependence of resistivity across the high-pressure, see Fig. 2, and high-temperature transition [6]. Since the high-temperature transition is associated with the charge delocalization, we conclude the same for the high-pressure transition. Upon applying pressure, the Mn-O bond distances are reduced, which induces an overlap of the Mn orbitals, and a change to an average valence $Mn^{3.25+}$. This causes the regularization of the MnO_6 octahedra and an overall symmetry increase. Given the similarity of the charge ordering transition in $CaMn_7O_{12}$, which occurs at 440 K at ambient pressure and at 295 K at the midpoint of 24 GPa, we estimate the slope of the phase boundary to be $dT_c/dp \approx -6$ K/GPa.

2. *X-ray diffraction at 70 K*

Below $T_{oo} = 250$ K $CaMn_7O_{12}$ develops an incommensurate structural modulation connected to the displacement of the O atoms, and effectively modulation of the Mn-O bond lengths [15] and thus an incommensurate orbital ordering [3]. Further on, below $T_{N1} = 90$ K, it hosts a helical, antiferromagnetic ordering which causes giant ferroelectricity of improper character, which attracted a lot of scientific interest. Since the magnetic and structural modulations in $CaMn_7O_{12}$ are closely connected [2,3,15], we were motivated to determine the pressure evolution of the structural modulations, with potential implications on the electronic properties.

In Fig. 5 we show the pressure evolution of a selected group of reflections. Figure 5(a) shows parts of the diffraction images collected upon rotating the sample in full ω range, which facilitates a qualitative comparison. The satellite reflections indicating the structural modulation are shown with red labels. Their intensity decreases with increasing pressure, as shown in Fig. 5(b), for the $(6\,\bar{5}\,1+\delta)$ reflection (black line) and the $(7\,\bar{5}\,3+\delta)$ reflection (red line). Due to small intensity of the satellite reflections we were not able to reliably index the satellite reflections above 15 GPa. However, qualitative comparison of images such as the representative ones in Fig. 5(a) suggests the modulation vector k remains unchanged with pressure as shown in Fig. 5(c), where δ stands for the z component of the modulation vector, i.e., $k = (0\,0\,\delta)$. For

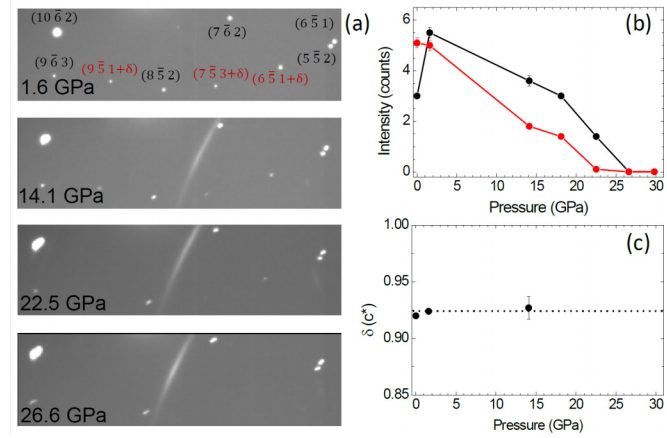

FIG. 5. (a) Section of the same x-ray diffraction image of a single crystal of $CaMn_7O_{12}$ at 70 K measured at different pressures. Labels close to the bright spots show the indices of the reflection, with the black labels corresponding to the main reflections, and the red labels to the satellite reflections. (b) Pressure dependence of the intensity of the $(7\,\bar{5}\,3+\delta)$ (red) and $(6\,\bar{5}\,1+\delta)$ (black) satellite reflections show the disappearance of the modulation around 25 GPa. (c) Pressure dependence of the z component of the modulation vector $k = (0\,0\,\delta)$.

displacive modulation of O atoms in $CaMn_7O_{12}$ the intensity of the satellite reflections corresponds to the amplitude of the displacement [35]. Thus, upon increasing pressure we observe a continuous decrease of the amplitude of the modulation, and the structure reenters the nonmodulated phase around 25 GPa, see Fig. 5(b).

The refinement of the average structure was successful up to the maximum pressure reached, 29.8 GPa, for which the refinement details are shown in Table I. Lattice parameters and unit cell volume do not show any discontinuities in the investigated pressure range, and the rhombohedral distortion remains around the value of 90.2°, see Fig. 4(c). Comparison of the values of lattice parameters at 295 and 70 K shows very small thermal expansion of the lattice, illustrated in Fig. 4(a), and previously reported for $CaMn_7O_{12}$ [2,15]. At the same time the average Mn-O bond lengths decrease linearly with pressure as shown in Fig. 6, and the suppression of the incommensurate phase at 25 GPa does not seem to affect the average Jahn-Teller distortion of the octahedra. Just as at ambient temperature, the compressibility of the long Mn^{3+}-O bond length is higher than that of the short Mn^{3+}-O bond length, and the extrapolation of the consequent Jahn-Teller distortion, see inset in Fig. 6, implies the regularization of the $Mn^{3+}O_6$ octahedra at 78 GPa, the value that is coincidentally the same as the one extrapolated from the data at ambient temperature. Overall, the evolution of the average structure of $CaMn_7O_{12}$ at 70 K is similar to ambient temperature, before the charge ordering transition. This was expected based on the extrapolation of the previously determined phase boundary of $dT_c/dp \approx -6$ K/GPa with $T_c = 440$ K at ambient pressure, which at 70 K places the charge ordering transition at ≈60 GPa, way above the measured pressure range. Additionally, the slope of the phase boundary between the incommensurate and charge ordered phase can be estimated from $T_{oo} = 250$ K at ambient pressure and $T_{oo} = 70$ K at 25 GPa to be $dT_{oo}/dp \approx -7.2$ K/GPa.

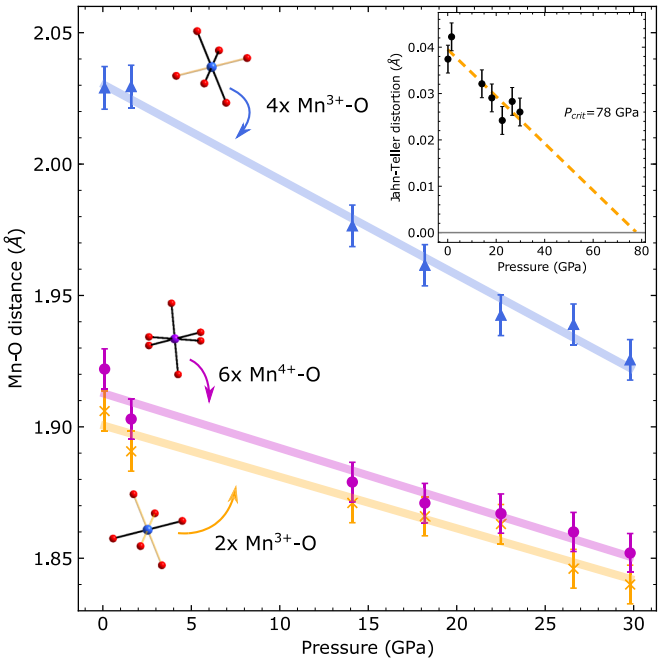

FIG. 6. Pressure dependence of the average Mn^{3+}-O and Mn^{4+}-O distances of $CaMn_7O_{12}$ obtained at 70 K. The four long Mn^{3+}-O, the two short Mn^{3+}-O, and the six Mn^{4+}-O distances are represented by circles, squares, and triangles, respectively, while the solid lines are guides for the eye. Inset shows the evolution of the Jahn-Teller distortion of the $Mn^{3+}O_6$ octahedra. The dashed line is a linear extrapolation of Jahn-Teller distortion.

IV. CONCLUSIONS

In summary, we have studied the Mn^{3+}/Mn^{4+} to $Mn^{3.25+}$ charge ordering phase transition of $CaMn_7O_{12}$ under compression by means of resistivity and single crystal x-ray diffraction. We have found that a resistivity drop of two orders of magnitude from 20 to 28 GPa is followed by a complete regularization of the $Mn^{3+}O_6$ octahedra and an increase of the overall symmetry from $R\bar{3}$ to $Im\bar{3}$. The pressure evolution of the crystal structure is continuous across the transition, suggesting its displacive character. This high-pressure transition is very similar to that previously obtained at ambient pressure and 440 K which allows us to determine the slope of the phase boundary of $dT_c/dp \approx -6$ K/GPa.

The single-crystal diffraction measurements performed at 70 K allowed us to follow the satellite reflections of the modulated multiferroic structure of $CaMn_7O_{12}$. The incommensurate modulation vanishes around 25 GPa, without any observable change in the modulation vector, where the $CaMn_7O_{12}$ sample reenters the nonmodulated structure observed at ambient conditions. In addition, the suppression of the incommensurate phase at 25 GPa does not seem to affect the average distortion of the octahedra.

We provide Supplemental Material with details of the crystal structure refinements [30].

ACKNOWLEDGMENTS

Y. Li and X. Du from Peking University are greatly acknowledged for growing and providing the $CaMn_7O_{12}$ crystals. D. Spahr and J. König from Goethe University are acknowledged for help with the single-crystal diffraction experiments. M.S. would like to acknowledge the financial support under the DFG-ANR Grant No. WI1232/41-1 and DFG GACR Project No. WI3320/3-1. V.M. and J.R.-F. thank the financial support from the Spanish Ministerio de Ciencia e Innovación (MICINN) for the Beatriz Galindo Program (BG20/000777) and for the Project No. PGC2018-097520-A-I00, respectively. DESY Photon Science is gratefully acknowledged. PETRA III at DESY is a member of the Helmholtz Association (HGF).

[1] G. Zhang, S. Dong, Z. Yan, Y. Guo, Q. Zhang, S. Yunoki, E. Dagotto, and J.-M. Liu, Phys. Rev. B **84**, 174413 (2011).
[2] R. D. Johnson, L. C. Chapon, D. D. Khalyavin, P. Manuel, P. G. Radaelli, and C. Martin, Phys. Rev. Lett. **108**, 067201 (2012).
[3] N. J. Perks, R. D. Johnson, C. Martin, L. C. Chapon, and P. G. Radaelli, Nat. Commun. **3**, 1277 (2012).
[4] X. Z. Lu, M. H. Whangbo, S. Dong, X. G. Gong, and H. J. Xiang, Phys. Rev. Lett. **108**, 187204 (2012).
[5] K. Gautam, D. K. Shukla, S. Francoual, J. Bednarcik, J. R. L. Mardegan, H.-P. Liermann, R. Sankar, F. C. Chou, D. M. Phase, and J. Strempfer, Phys. Rev. B **95**, 144112 (2017).
[6] I. O. Troyanchuk, L. S. Lobanovsky, N. V. Kasper, M. Hervieu, A. Maignan, C. Michel, H. Szymczak, and A. Szewczyk, Phys. Rev. B **58**, 14903 (1998).
[7] A. Asamitsu, Y. Tomioka, H. Kuwahara, and Y. Tokura, Nature (London) **388**, 50 (1997).
[8] Y. Tomioka, A. Asamitsu, H. Kuwahara, Y. Moritomo, and Y. Tokura, Phys. Rev. B **53**, R1689(R) (1996).
[9] H. Matsuzaki, H. Uemura, M. Matsubara, T. Kimura, Y. Tokura, and H. Okamoto, Phys. Rev. B **79**, 235131 (2009).
[10] B. Bochu, J. C. Joubert, and M. Marezio, J. Solid State Chem. **11**, 88 (1974).
[11] A. Huon, A. C. Lang, D. Saldana-Greco, J. S. Lim, E. J. Moon, A. M. Rappe, M. L. Taheri, and S. J. May, Appl. Phys. Lett. **107**, 142901 (2015).
[12] S. M. Souliou, Y. Li, X. Du, M. Le Tacon, and A. Bosak, Phys. Rev. B **94**, 184309 (2016).
[13] C. Toulouse, C. Martin, M.-A. Measson, Y. Gallais, A. Sacuto, and M. Cazayous, Phys. Rev. B **99**, 024303 (2019).
[14] R. Przeniosło, I. Sosnowska, E. Suard, A. Hewat, and A. N. Fitch, J. Phys.: Condens. Matter **14**, 5747 (2002).
[15] W. Sławiński, R. Przeniosło, I. Sosnowska, and A. Chrobak, J. Phys. Soc. Jpn. **81**, 094708 (2012).
[16] J. Ruiz-Fuertes, O. Gomis, A. Segura, M. Bettinelli, M. Burianek, and M. Mühlberg, Appl. Phys. Lett. **112**, 042901 (2018).
[17] J. Ruiz-Fuertes, T. Bernert, D. Zimmer, N. Schrodt, M. Koch-Müller, B. Winkler, L. Bayarjargal, C. Popescu, S. MacLeod, and K. Glazyrin, Phys. Rev. B **96**, 094101 (2017).

[18] G. A. Samara, T. Sakudo, and K. Yoshimitsu, Phys. Rev. Lett. **35**, 1767 (1975).
[19] R. Boehler, Rev. Sci. Instrum. **77**, 115103 (2006).
[20] H. K. Mao, J.-A. Xu, and P. M. Bell, Geophys. Res.: Solid Earth **91**, 4673 (1986).
[21] H.-P. Liermann, Z. Konopkova, W. Morgenroth, K. Glazyrin, J. Bednarcik, E. E. McBride, S. Petitgirard, J. T. Delitz, M. Wendt, Y. Bican *et al.*, J. Synchrotron Rad. **22**, 908 (2015).
[22] Agilent, Crysalis^{Pro} software system, version 1.171.36.28 (Agilent Technologies UK Ltd., Oxford, UK, 2013).
[23] G. M. Sheldrick, Acta Crystallogr. Sect. A **71**, 3 (2015).
[24] G. M. Sheldrick, Acta Crystallogr. Sect. C **71**, 3 (2015).
[25] Interested parties are encouraged to contact us in case of requiring further details about the sample preparation for the resistivity measurements.
[26] D. Spahr, M. Stekiel, D. Zimmer, L. Bayarjargal, K. Bunk, W. Morgenroth, V. Milman, K. Refson, D. Jochym, P. J. P. Byrne *et al.*, Acta Crystallogr. Sect. B **76**, 979 (2020).
[27] W. Massa and M. Steiner, J. Solid State Chem. **32**, 137 (1980).
[28] M. Molinier and W. Massa, Z. Naturforsch. Teil B **47**, 783 (1992).
[29] J. Ruiz-Fuertes, A. Friedrich, J. Pellicer-Porres, D. Errandonea, A. Segura, W. Morgenroth, E. Haussühl, C.-Y. Tu, and A. Polian, Chem. Mater. **23**, 4220 (2011).
[30] See Supplemental Material at http://link.aps.org/supplemental/10.1103/PhysRevB.105.064110 for details on the crystal structure refinement, which includes Ref. [36].
[31] $\alpha_c = \text{acos}(\frac{1-\frac{3}{8}(a_R/c_R)^2}{1+\frac{3}{4}(a_R/c_R)^2})$. α_c is the pseudocubic angle, and a_R, c_R are the rhombohedral lattice parameters.
[32] F. Birch, Phys. Rev. **71**, 809 (1947).
[33] F. Aguado, F. Rodríguez, R. Valiente, J.-P. Itie, and M. Hanfland, Phys. Rev. B **85**, 100101(R) (2012).
[34] F. Rodríguez and F. Aguado, J. Chem. Phys. **118**, 10867 (2003).
[35] T. Janssen, A. Janner, A. Looijenga-Vos, and P. M. de Wolff, Incommensurate and commensurate modulated structures, in *International Tables for Crystallography* (International Union of Crystallography, 2006), Vol. C, Chap. 9.8, pp. 907–955.
[36] A. A. Ramadan, R. D. Gould, and A. Ashour, Thin Solid Films **239**, 272 (1994).